2015

Interfacial reactions of a MAX phase/superalloy hybrid

James L. Smialek
NASA Glenn Research Center, james.l.smialek@nasa.gov

Anita Garg
National Aeronautics and Space Administration

Research article

SURFACE and INTERFACE ANALYSIS

Received: 8 March 2015 Revised: 13 May 2015 Accepted: 13 May 2015 Published online in Wiley Online Library: 29 June 2015

(wileyonlinelibrary.com) DOI 10.1002/sia.5784

Interfacial reactions of a MAX phase/superalloy hybrid

James L. Smialek* and Anita Garg

Oxidation resistant, strain tolerant MAX phase coatings are of general interest for high temperature applications. Accordingly, Cr_2AlC MAX phase coupons were vacuum diffusion bonded to an advanced turbine disk alloy at 1100 °C for compatibility studies. The interface revealed an inner diffusion zone consisting of ~10 μm of β-Ni(Co)Al, decorated with various γ′ $(Ni,Co)_3Al$, Ta(Ti,Nb)C, and $W(Cr,Mo)_3B_2$ precipitates. On the Cr_2AlC side, an additional ~40-μm Al-depletion zone of Cr_7C_3 formed an interconnected network with the β-Ni(Co)Al. On the superalloy side, enhanced carbide precipitation developed over a depth of ~80 μm. Subsequent annealing for 100 h and 1000 h at 800 °C coarsened some features, enhanced TCP precipitation in the superalloy, but only enlarged the diffusion layers by ~5 μm at most. Because of Al depletion from the MAX phase and corresponding Al enrichment of the alloy, the reaction zone displayed similarities to an oxidized Cr_2AlC surface and an aluminized superalloy, respectively. Published 2015. This article is a U.S. Government work and is in the public domain in the USA.

Keywords: Cr_2AlC MAX phase; diffusion reaction; superalloys; aerospace materials; high temperature; coatings

Introduction

M–A–X compounds are carbide or nitride ceramics well known for their unique behavior as 'deformable' and 'strain-tolerant' ceramics. This property arises from the special hexagonal crystal structure that contains weakly bonded (0003) hkil crystallographic planes.[1,2] This allows these compounds to deform by sliding and kinking in contrast to macroscopic cracking and cleavage typical of most ceramics. The chemistry is generically described as M = group III–VI transition metals (Sc, Ti, V, Cr); A = group IIIA–VA (Al, Si, Ge, P); and X = C, N. The stoichiometry is commonly M_2AX, M_3AX_2, or M_4AX_3. The structure is distinguished by planes of A-group elements every 3rd, 4th, or 5th layer, respectively, in a global $M_{n+1}X_n$ lattice. While many of the M–X ceramic properties are maintained, such as high melting, high modulus, and high strength, the relatively weak M–A and A–X bonds allow for easy intercalated planar delamination that results in the high strain tolerance. This produces unique aspects such as good machinability, moderate fracture toughness, excellent thermal fatigue resistance, and high coefficient of thermal expansion for an otherwise 'ceramic-like' material.

While there have been over 60 MAX phases identified, those containing Al have the potential of excellent oxidation resistance owing to the formation of Al_2O_3 scales.[3] These include primarily Ti_2AlN, Ti_3AlC_2, Ti_2AlC, and Cr_2AlC exhibiting the highest oxidation resistance.[4–6] In general these studies have found alumina scale growth rates in the range of those formed on oxidation resistant NiAl or FeCrAl alloys, with good oxidation resistance up to 1200 °C for Cr_2AlC and 1300 °C for Ti_3AlC_2 and Ti_2AlC.[3] Indeed, rate controlling oxygen grain boundary diffusion in the scale has been surmised to be equivalent to that observed for oxidation resistant FeCrAl alloys.[7,8] Ti_2AlC has been characterized as having good cyclic oxidation resistance because of its good thermal expansion match to that of the alumina scale. The higher CTE of Cr_2AlC leads to an increased spallation tendency similar to that observed for metals, but at higher temperatures.

Furthermore, published studies document good corrosion resistance of Ti_3AlC_2 and Cr_2AlC in SO_2 environments.[9,10] Molten Na_2SO_4 salt hot corrosion resistance was demonstrated for Cr_2AlC,[5] and for preoxidized Ti_2AlC[11] and Ti_3AlC_2.[12] Thus the production of MAX phases as protective coatings for stainless steel, Ni-base superalloy M38G, Ti6242, and TiAl substrates has been demonstrated, primarily via magnetron sputtering.[2,13–18]

Emerging problem areas of environmental degradation in turbines are gas phase embrittlement, oxidation, and low temperature hot corrosion (LTHC) of advanced disk alloys used in the high pressure turbine stage.[19–27] This issue becomes more critical at the highly stressed disk and blade attachment regions. Accordingly, crack tip oxidation has experienced in-depth attention.[28,29] Typical metallic aluminide and NiCrAlY coatings, engineered for higher temperature blade exposures and Type II hot corrosion resistance, actually lead to fatigue debits because of CTE mismatch stresses, lower strength, and tendencies for brittle behavior in a disk environment. This has led to modified approaches, such as fully ductile Ni–Cr coatings or fatigue resistant, refractory strengthened γ/γ′ NiCrAl–Ta,W 'EQ' coating alloys.[30,31]

In the present study, we consider Cr_2AlC in a potential coating application for thermal protection in gas turbine engines. It has three desirable attributes: strain tolerance because of microlaminate kinking, a relatively high CTE (13×10^{-6}/°C), and good Type I hot corrosion resistance.[5] Initial studies indicate improved Type II low temperature corrosion behavior as well [J. Smialek, unpublished research]. However little information is available regarding cyclic thermal stability of a superalloy coated with this

* Correspondence to: James L. Smialek, National Aeronautics and Space Administration, Glenn Research Center, Cleveland, OH 44135, USA.
E-mail: james.l.smialek@nasa.gov

National Aeronautics and Space Administration, Glenn Research Center, Cleveland, OH, 44135, USA

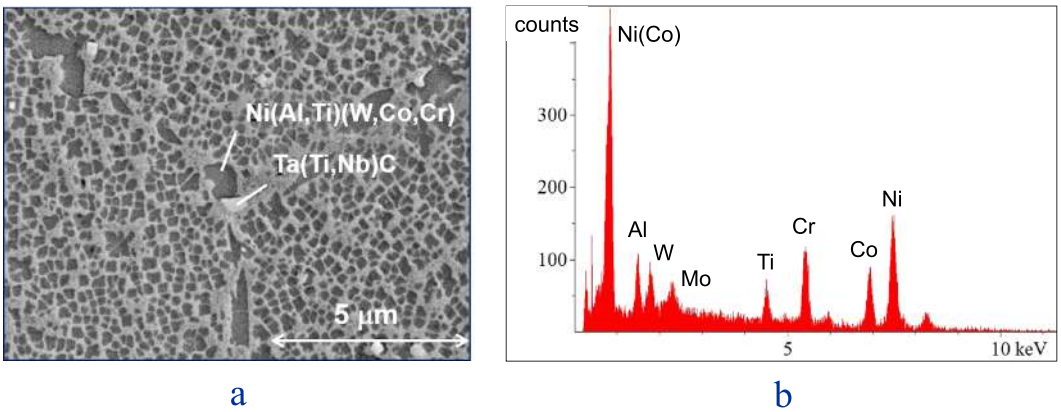

Figure 1. Unaffected LSHR superalloy features away from the interface: a) fine–cuboidal γ′ particles in a γ matrix, grain boundary γ′, and MC carbides; b) EDS spectra corresponding to overall γ/γ′ region showing high Ni, Co, and Cr peaks, with Al, Ti, W, Ta, and Nb. (sample DC2, exposed 100 h at 800 °C; SEM/SE).

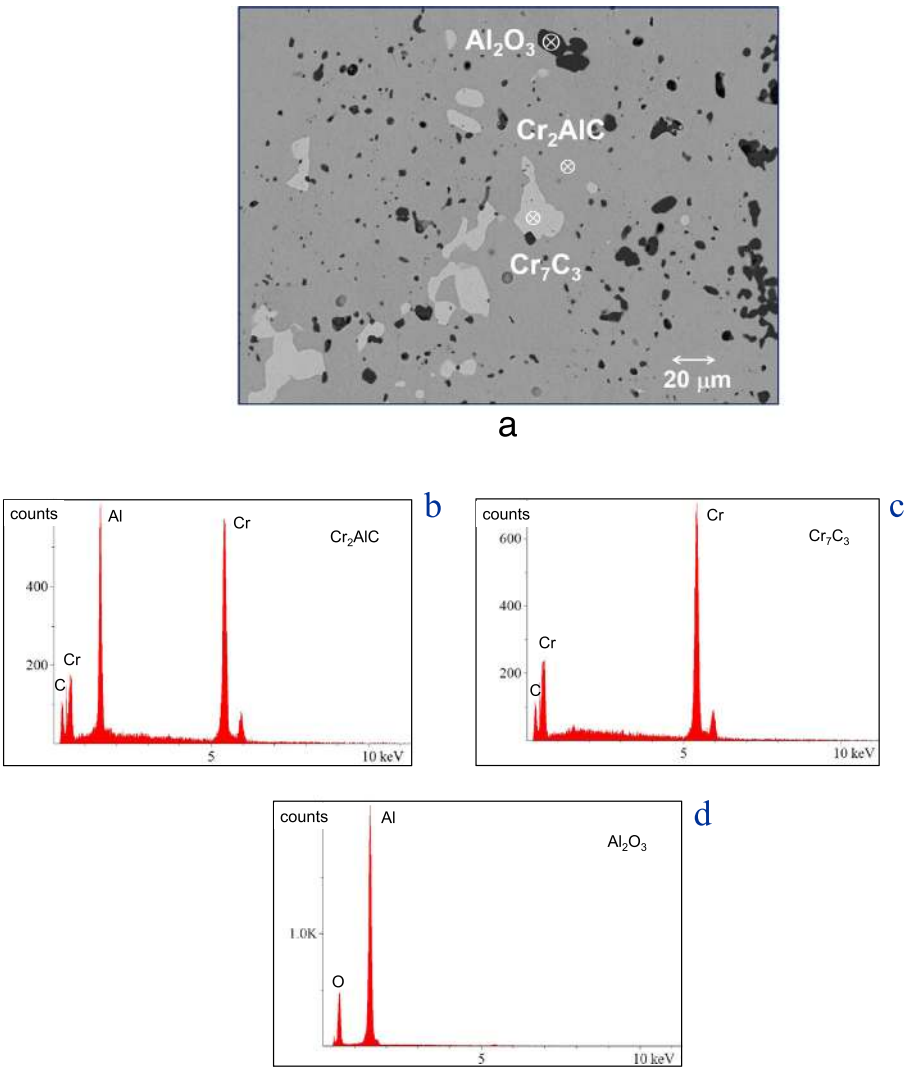

Figure 2. Unaffected Cr_2AlC MAX phase structure away from the interface: a) ~5 vol. % Al_2O_3 (dark) and 3 vol. % Cr_7C_3 (bright) impurity phases; EDS spectra corresponding to b) Cr_2AlC MAX phase; c) Cr_7C_3; and d) Al_2O_3 impurity phases. (Sample DC2, exposed 100 h at 800 °C; SEM/BSE).

material. Thus the purpose of the present paper is to examine the compatibility of a hot pressed Cr_2AlC–superalloy hybrid after repeated cycling to 800 °C. Interfacial mechanical and diffusional stabilities are the primary focus points of the present work, whereas many preliminary results, including scale characterizations, can be found in prior work.[32]

Materials and procedure

The superalloy portion of the hybrid couple was a low γ′ solvus and a high refractory content alloy, called 'LSHR', developed by NASA for disk applications.[33] The as-forged LSHR composition is (wt.%):

Ni-20.4Co-12.3Cr-4.3W-3.4Ti-3.4Al-
2.7Mo-1.5Ta-1.5Nb-0.05Zr-.03B-.04C.

Production scale powder metallurgy disks were produced by argon atomized and hot compacted powders, followed by extrusion and isothermal forging. Specimen blanks were supersolvus heat treated at 1171 °C for 2 h, cooled at 72°/min., and dual aged at 855 °C/4 h and 775 °C/8 h. Phase constituents were primarily γ-Ni(-Co,Cr,Mo,W) solid solution, strengthened by dense γ′-Ni(Ti,Ta,Nb)$_3$Al cuboidal precipitates. The alloy also contained a low density of dispersed (Ta,Nb,Ti)C carbides, coarse (W,Mo,Cr)$_3$B$_2$ borides, and fine grain boundary (W,Cr)$_{23}$C$_6$ carbide particles.[34] A representative microstructure including a grain boundary and the EDS spectrum corresponding to the general γ/γ′ area are presented in Fig. 1(a,b).

The starting Cr_2AlC MAX phase ingot, approximately 2 × 2 × 12 cm, was obtained from Sandvik/Kanthal. The as-received density was ~67% based on an assumed theoretical density of 5.22 g/cm^3. Thus an effort was made to improve density by hot pressing in vacuum (77 Pa or 10^{-6} Torr) using graphite dies. It was found that hot pressing at 1300 °C for 2 h using 35 MPa pressure resulted in 97% density. Numerous fine secondary phases were present as shown in Fig. 2. The phase constituency was estimated by XRD Rietveld analyses to be ~92% Cr_2AlC, 5% Al_2O_3, and 3% Cr_7C_3 (vol. %). (This did not change appreciably in bulk with 1300 °C hot pressing, 1100 °C diffusion bonding, or 800 °C thermal exposures). The corresponding EDS spectra for the MAX phase constituents are presented in Figs. 2b–2d. They show the distinguishing peaks of the constituent Cr_2AlC matrix and Al_2O_3 and Cr_7C_3 impurity phases.

Coupons ~6 mm by 12 mm were sectioned from the LSHR superalloy and hot pressed Cr_2AlC using a diamond wafer saw. The thickness of the two LSHR coupons was 1.8 mm, whereas the Cr_2AlC coupons were ~0.3 and 1.5 mm for the 100-h and 1000-h exposure couples (samples DC2 and DC3), respectively. These were polished to 2400 grit SiC emery finish. Bonding was accomplished by vacuum hot pressing at 1100 °C for 2 h under ~110-MPa pressure (DC2). This caused substantial deformation of the LSHR alloy, to the extent that the slightly undersized Cr_2AlC layer was fully impressed into the metal. The second couple (DC3), hot pressed at 1100 °C for 2 h at ~52 MPa pressure, was used for the 1000 h test. Here, only minimal deformation of the LSHR alloy was noted, as shown in Fig. 3. Grafoil mold release was burned off at 800 °C for 1 h. One end of the couple was sectioned for as-diffusion bonded microscopy as a baseline for comparison to the thermally cycled samples.

The cut edge and major 6 × 12 mm exposed surfaces were re-polished to 4000 grit emery and ultrasonically cleaned in ethanol. The couples, and separate coupons of LSHR and Cr_2AlC, were exposed to 800 °C air in a Thermolyne resistance muffle furnace, with intermittent removal for weight change measurements and optical examination. Vacuum infiltrated epoxy mounted and polished cross sections were prepared before and after oxidation. These sections were analyzed by conventional metallographic, X-ray diffraction (XRD), and scanning electron microscopy (SEM) techniques. SEM samples were coated with a conductive carbon coating and imaged primarily in backscatter electron imaging mode (BSE), sensitive to atomic weight of the features. Energy dispersive

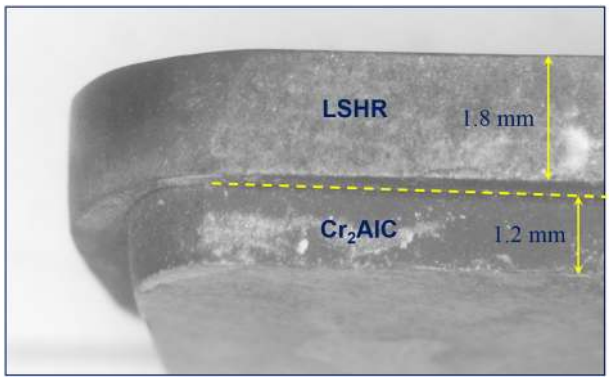

Figure 3. Macrophoto of hot pressed LSHR/Cr_2AlC hybrid couple showing good bonding with minimal deformation (sample DC3, 1100 °C, 2 h, ~**50** MPa).

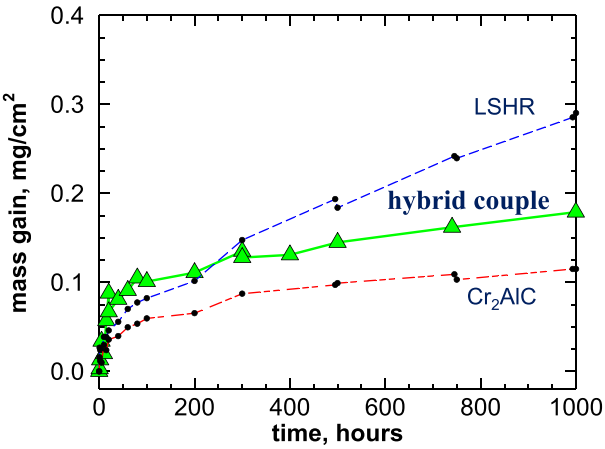

Figure 4. Mass gain for interrupted 800 °C oxidation of hybrid couple DC3. Corresponding results for separate LSHR and Cr_2AlC samples indicate higher and lower mass gains, respectively. All indicate low oxygen pickup, i.e. less than 0.5 mg/cm^2 after 1000 h.

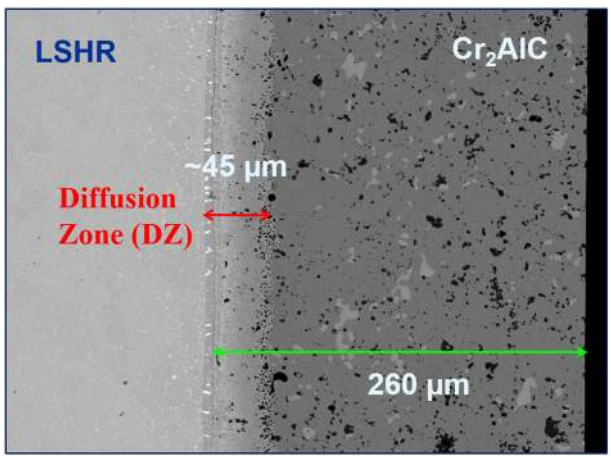

Figure 5. Polished cross-sectional slice of the hybrid couple after hot pressing (sample DC2, hot pressed 1100 °C, 2 h, ~100 MPa). SEM/BSE shows inner diffusion zone (middle) and full thickness of the three-phase Cr_2AlC layer on the right.

spectroscopy (EDS) was conducted at 15 kV for chemical composition, with selective standardless semi-quantitative analysis. But because of the carbon coating, fine particle sizes, and excited volume overlap issues, most EDS assessments of phases were qualitative.

Results

The 800 °C weight change behavior of the diffusion bonded hybrid couple DC3 is shown in Fig. 4. Very little oxidation occurred, gaining only 0.18 mg/cm^2 after 1000 h. The companion sample DC2 gained 0.09 mg/cm^2 after 100 h, as shown previously.[32] Both the Cr_2AlC and LSHR alloy contribute to this 1000-h value, with separate individual samples gaining 0.12 and 0.29 mg/cm^2, respectively. The literature suggests 800 °C weight changes on the order 0.20 mg/cm^2 for Cr_2AlC oxidized for 1000 h[5] and 0.57 mg/cm^2 for LSHR oxidized for 1000 h.[35] Because oxidation is not a focus of this particular study, the kinetics are not discussed in more detail. There were no signs of delamination or oxidative deterioration of the bond interface after hot pressing or intermittent cycling to 800 °C.[32]

The full thickness of the Cr_2AlC layer of the as hot-pressed DC2 sample can be seen to be on the order of 260 μm, with an overall diffusion zone of ~45 μm, as presented in Fig. 5. The original 300-μm Cr_2AlC coupon was reduced to a 260-μm-thick Cr_2AlC layer after removing ~40 μm by surface preparation after hot pressing. Unaffected LSHR superalloy and unaffected Cr_2AlC structures can be seen at the extreme left and right regions, respectively. An overview of the major diffusion zones can be represented by the montage presented in Fig. 6, obtained for the DC2 sample after 100 h at 800 °C. Here and under all conditions the LSHR region exhibits a gradation of white particles, with increased size and frequency near the bonded interface. The Cr_2AlC side exhibits a distinctive diffusion layer along with numerous other features. These

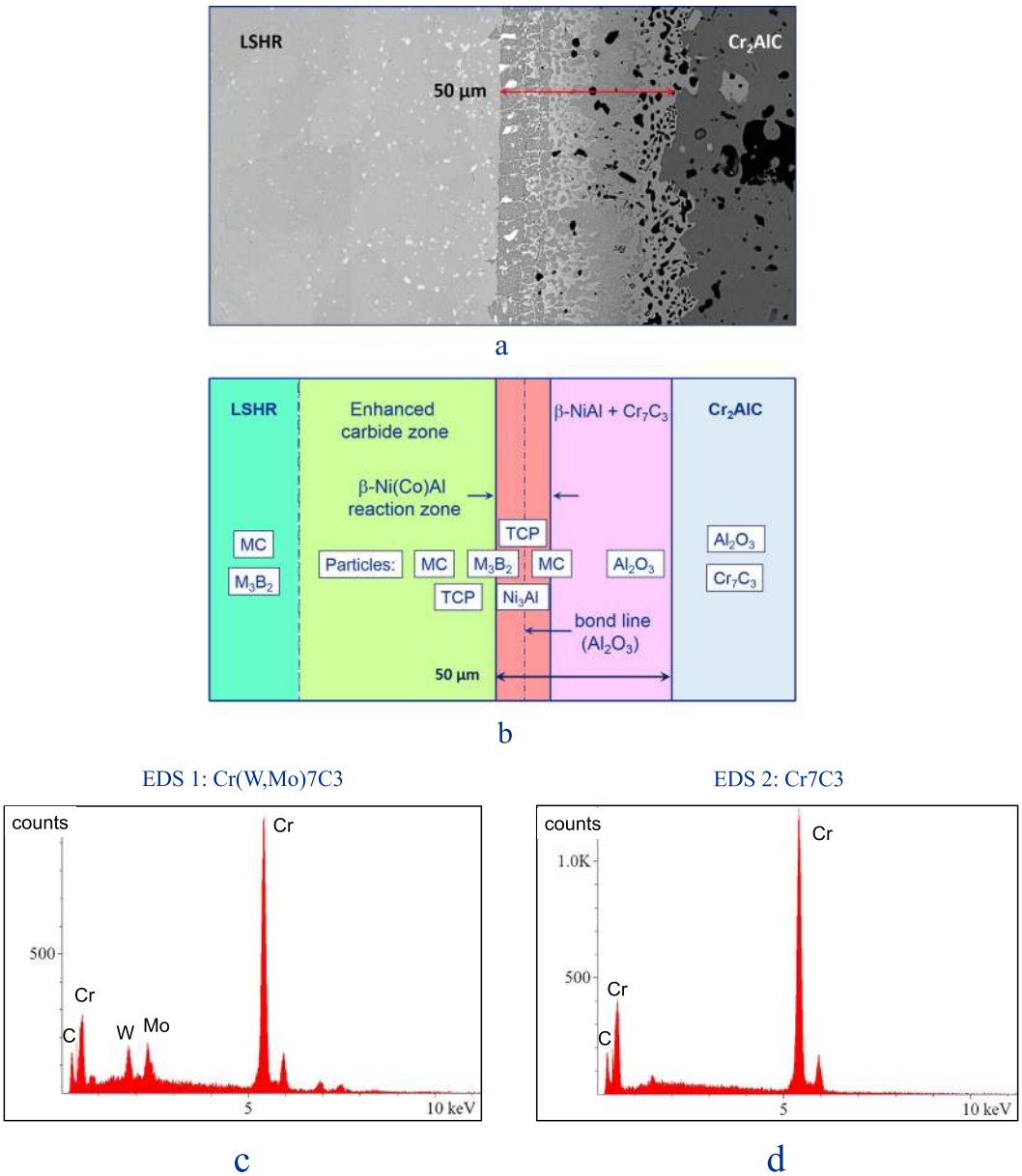

Figure 6. Complete diffusion zone for sample DC2 after 100-h exposure at 800 °C. a) SEM/BSE image; b) schematic illustrating location of phases observed; EDS spectra corresponding to c) Cr_7C_3 (with W, Mo) near interface, and d) pure Cr_7C_3 near Cr_2AlC MAX phase.

are summarized in the schematic of Fig. 6b that can be used as a microstructural guide in the following discussion of the specific details. Furthermore, a comprehensive complementary catalog of all the phases found in each of these distinctive zones is presented in the Appendix, Table A1.

The details of the diffusion zone features and their chemistries are discussed for the different conditions in the remaining figures. The microstructure of the DC2 sample after hot pressing is presented in Fig. 7a. Energy dispersive spectroscopy suggested that the primary reaction layer is β-Ni(Co)Al (Fig. 7b), peppered with less distinct very fine precipitates. Typically, semi-quantitative analyses yielded 42Ni–38Al–13Co–5Cr–2Ti (at. %) for all the regions marked β-Ni(Co)Al.

The center bond line is decorated with dark Al_2O_3 particles (Fig. 7c). The origin of the Al_2O_3 is unclear, but likely occurred by slight oxidation in the hot press. In the diffusion zone close to the superalloy side, large and very bright $W(Mo,Cr)_3B_2$ (Fig. 7d) particles were commonly observed. (Note: B peaks are problematic in SEM/EDS analyses). On the other hand, light gray (Ta,Nb,Ti)C particles (Fig. 7e) were prevalent on both sides of the bond line. Both of these boride and carbide phases were more pronounced in these regions as compared to the unaffected superalloy region far away from the interface, also with size and shape differences. The suggested boride and carbide stoichiometries derive from published precise TEM diffraction, microprobe, and semi-quantitative EDS analyses of similar features in the same bulk superalloy.[34] The latter study indicated 33.0Cr–20.6Co–14.3Ni–5.4Mo–2.5W–24.2C in atomic percent for the MC carbide and 18.8Cr–15.8Mo–8.7W–39.7B (plus 4.5Ni–3.2Co–2.4Nb–2.4Ti–0.7Ta–3.8C) atomic percent for the M_3B_2 boride.[34] A high density of fine precipitates was observed in the primary reaction zone β matrix (Fig. 7a), but were too narrow (~0.2 μm) for EDS analysis. Moving to the right side of the diffusion zone, closer to the Cr_2AlC wafer, extensive growth of an amorphic Cr_7C_3 phase was observed intertwined with the β-Ni(Co)Al.

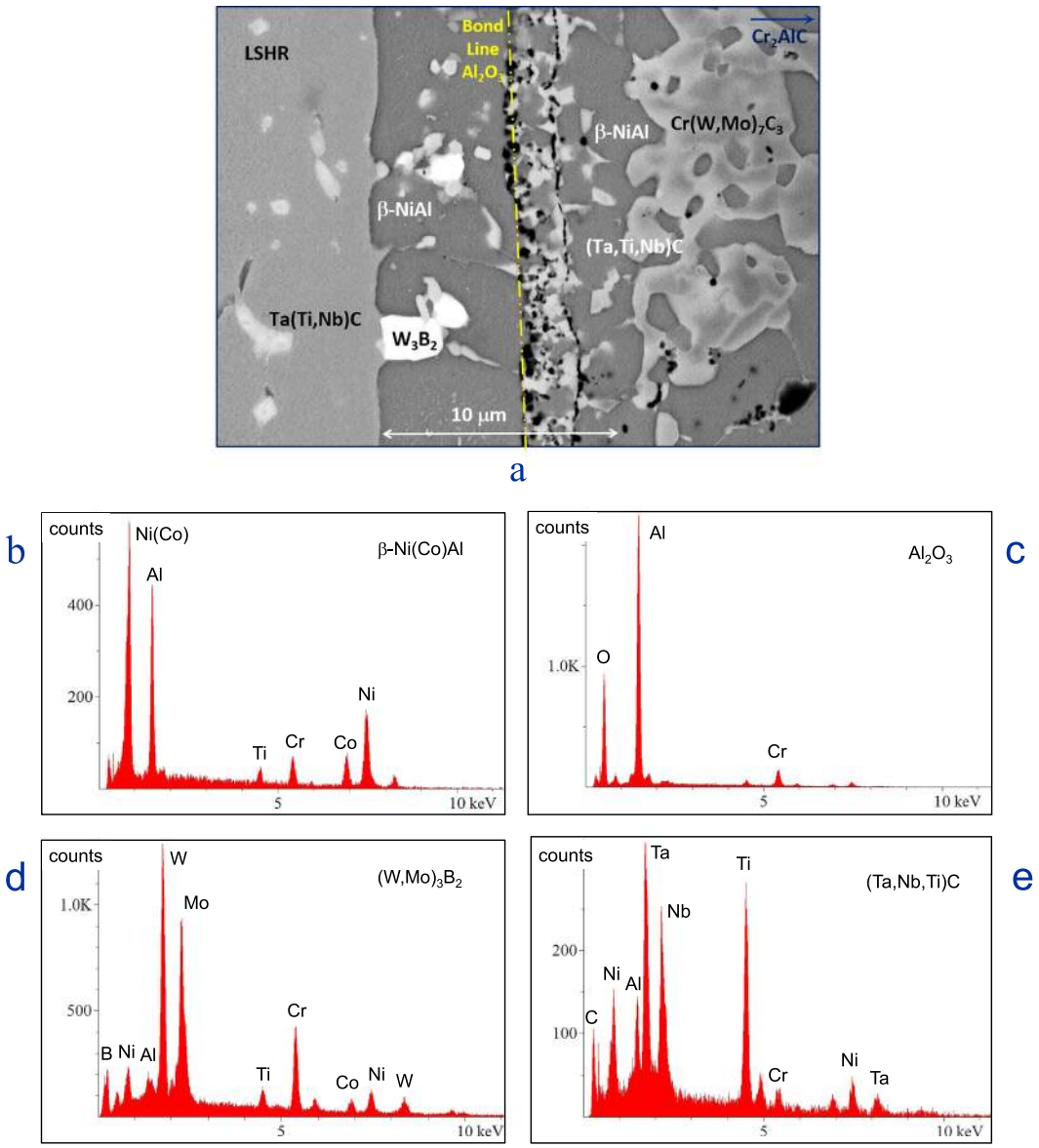

Figure 7. Detailed microstructural features of the diffusion/reaction zones for as-hot pressed sample DC2 showing a) Ni(Co)Al reaction layer with bright M_3B_2, light MC, γ′, and dark Al_2O_3 bond-line particles; EDS spectra corresponding to b) Ni(Co)Al reaction layer, c) embedded Al_2O_3, d) (W, Mo, Cr)$_3B_2$ borides, and e) (Ta, Ti, Nb)C carbides.

SURFACE and INTERFACE ANALYSIS

After sample DC2 was heated for 100 h at 800 °C, the interface displayed features similar to those observed after hot pressing. The β layer has grown by approximately 3 μm. In the LSHR region adjacent to the diffusion interface, nucleation of a new phase with long, needle-like or platelet morphology has begun. The fine precipitate phase in the β-Ni(Co)Al interdiffusion layer coarsened into more distinctly visible intragranular precipitates arranged in a Widmanstätten pattern (Fig. 8a). EDS analysis (Fig. 8b) suggested these and larger precipitates in the region to be high in Ni, Co, Al, and Cr. These spectra are similar to those for γ′-Ni_3Al, but with higher Cr sometimes approaching that of σ-phase TCP (previously measured as 28Co–26Cr–14Mo–14W–12Ni–4Ta–2Ti in the alloy, but without any Al[34]). Semi-quantitative standardless EDS analyses yielded 26Ni–20Al–22Co–27Cr–2Mo–2W–1Ti (at. %) for a larger one of these questionable particles having the highest Cr level.

The Cr_7C_3 phase is interspersed with β-Ni(Co)Al, but extends out of this field of view. Closer to the bond line, as shown in the wide field montage of Fig. 6a, the Cr_7C_3 phase contained small amounts of W and Mo from the superalloy (Fig. 6c). These elements were absent near the Cr_2AlC interface (Fig. 6d), where Cr_7C_3 developed into almost a continuous layer. This layer also contained a higher concentration of large Al_2O_3 particles as compared those present in the interior of the Cr_2AlC coupon (Fig. 6a).

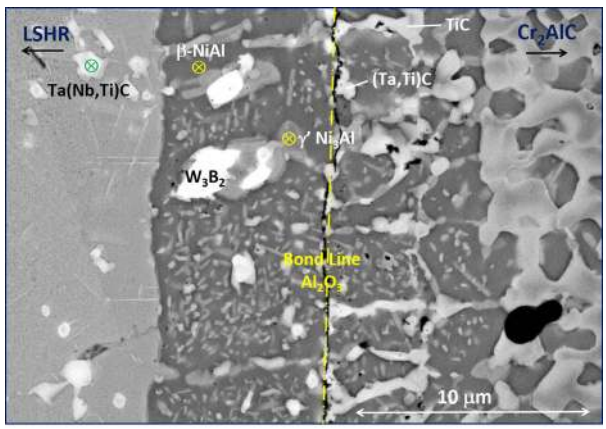

a

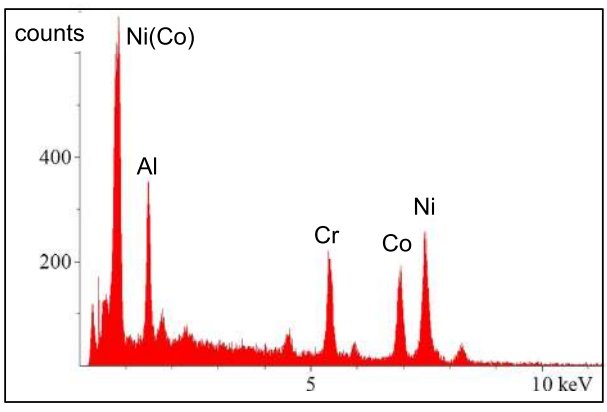

b

Figure 8. Detailed microstructural features of the diffusion/reaction zones for sample DC2 after 100-h exposure at 800 °C showing a) dense Widmanstätten phase in NiAl, and b) corresponding EDS spectrum showing high Ni, Al peaks (with Cr, Co) for the fine Ni(Co)Al reaction zone particles.

Finally, after 1000 h at 800 °C (sample DC3, Fig. 9), many of the features present in Fig. 8a had coarsened substantially. Most prominent was the coarsening of the fine Widmanstäten in the β-Ni(Co)Al layer adjacent to the superalloy, changing from fine to more equiaxed larger particles. No bond line Al_2O_3 particles were observed here or in the as-hot pressed microstructure, possibly because of a different pressure/temperature ramp schedule for this sample. Therefore the original interface could only be estimated based on similarities with the previous sample. In the LSHR region adjacent to the interface, the number density and size of the needle-like TCP phase had increased substantially. A new elliptical phase morphology now appeared in this region. Both regions were found to be rich in Co, Cr, Mo, W, and Ni (Fig. 9b) and are likely to be the Topologically Closed Packed (TCP) phase, similar to those reported in the literature for this alloy at 27.6Co–26.1Cr–14.2Mo–14.0W–11.7Ni–4.1Ta–2.4Ti in atomic percent.[34] In addition, darker particles were also distinctly visible at the grain boundaries in the LSHR. A characteristic EDS spectrum of the latter phase (Fig. 9c) suggested these particles to be a Cr(Mo,W)–oxide, possibly Cr(Mo,W)O_4. The other previously discussed phases such as MC and γ/γ′ are also marked in Fig. 9a. Despite these alterations, the individual and total overall diffusion zones did not increase with respect to the as-hot pressed dimensions (Table 1) as surmised from both low and high magnification measurements. These zones did not show a systematic increase in thickness compared to the DC2 100 h data either.

Discussion

Wafers of Cr_2AlC MAX phase have been successfully bonded to an advanced disk alloy, LSHR, at 1100 °C. A noticeable amount of interdiffusion took place during hot pressing, producing a distinct Ni–Al interfacial layer, consistent with β-Ni(Co)Al. This zone straddled what appeared to be the original interface, as demarked by alumina stringers in one sample. Little growth took place after 100 or 1000 h exposure to 800 °C ambient air. No evidence of interfacial damage or cracking was apparent despite cooling to room temperature for 10–20 times, respectively.

The reaction zone constituents can be described in terms of superalloy elements (Ni, Ta, Ti, W, Mo, and Nb) diffusing into the Cr_2AlC and counterdiffusion of MAX phase elements (Cr, Al, and C) moving into the superalloy. The inner reaction zone of β-Ni(Co)Al is a result of Al diffusing into the superalloy on one side and Ni diffusing into the MAX phase on the other, delineated in one sample by the Al_2O_3 at the original bond line. Many of the features in the reaction zone are reminiscent of microstructures formed in aluminized superalloys, both as-coated and after subsequent thermal exposure. Here, duplex microstructures were the rule, with an outer layer of β-NiAl and an inner layer containing γ′-Ni_3Al precipitates plus carbides.[36] Subsequent interdiffusion depletes the coating of Al and allows γ′-Ni_3Al precipitation within the β-phase.[37–39] Similarly, in the present study, various modifications of the interface zone were manifested on both sides of the bond line as (Ta, Ti, Nb)C carbide particles and a profusion of (Ni, Co, Al, Cr)-rich Widmanstätten precipitates, with compositions intermediate between the superalloy and the β-NiAl phase. W-rich M_3B_2 particles appeared exclusively on the LSHR side of the reaction zone.

The LSHR alloy adjacent to the diffusion zone exhibited a dispersion of σ-like TCP lathes after long time exposures, superimposed on the prior broad, fading zone of enlarged MC carbides. The

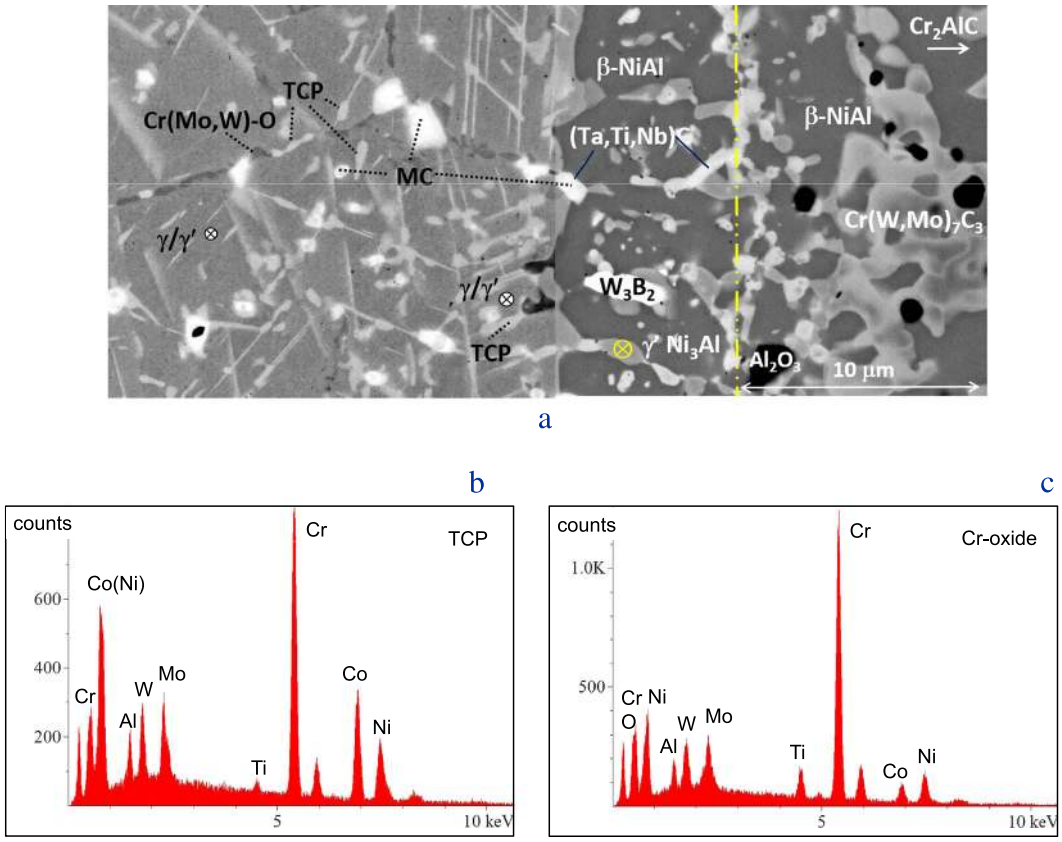

Figure 9. Detailed microstructural features of diffusion/reaction zones in sample DC3 after 1000-h exposure at 800 °C showing a) coarsened particulates in Ni(Co)Al layer and pronounced TCP platelet formation in the adjoining LSHR. Representative EDS spectra showing: b) high Cr peak in TCP platelets, and c) high Cr, O peaks in LSHR grain boundary phase.

Table 1. Diffusion layer thicknesses (μm) for hot pressed LSHR-Cr_2AlC, after hot pressing at 1100 °C and 800 °C exposures

	LSHR Carbide	LSHR β-NiAl	Cr_2AlC β-NiAl	Cr_2AlC Carbide	ΔDZ
Hot pressed DC2, 1100 °C, 4 h	81	5.8	5.4	33.9	—
Oxidized DC2, 800 °C, 100 h	78	7.2	6.8	35.8	+4.7
Hot pressed DC3, 1100 °C, 2 h	(60–90)	8.9	7.9	37.5	—
Oxidized DC3, 800 °C, 1000 h	83	6.4	6.4	36.3	−5.2

carbide enhancement and high-Cr TCP precipitates were consistent with C and Cr diffusing into the superalloy from the Cr_2AlC MAX phase. Again, Cr, Co, Mo, and W-rich TCP precipitates, such as σ, μ phases, are well-known occurrences in a similar zone beneath the external coating for annealed aluminized superalloys.[39,40] Also, fine alumina particles, similar to those found at the bond line in the present study, are sometimes seen trapped near the interface between the outer β-NiAl layer and inner diffusion zone in aluminized coatings.[38]

On the other side of the interface, i.e. toward the Cr_2AlC wafer, a multiphase zone with a large component of Cr-carbide has formed. This is analogous to similar Cr_7C_3 sublayer depletion zones formed under alumina scales as Al is extracted from Cr_2AlC during oxidation.[5,6] Also, it has been predicted thermodynamically and shown experimentally that NiAl will deplete Al from Cr_2AlC to form Cr_7C_3.[41] Given that Al in Cr_2AlC interdiffused with the nickel superalloy, Cr_7C_3 is an expected depletion zone in this LSHR–Cr_2AlC couple. Finally, some W, Mo, Ni, and Co have been observed in the Cr_7C_3 phase at the innermost region of the reaction layer, showing the limited extent of diffusion of these elements from the superalloy.

The degree of oxidation indicated by weight change was minimal. Oxidation was not a focus of this paper, but in general Cr_2O_3 and $(Cr,Ta,Ti)O_2$ rutile phases were identified on LSHR by xrd, while α-Al_2O_3 and α-Cr_2O_3 were identified for the Cr_2AlC MAX phase. At present, more detailed characterizations of these materials can be found in previous works.[21,32]

Conclusions

Cr_2AlC MAX phase is relatively stable, mechanically and chemically, with a Ni-base superalloy in 800 °C cycling and may offer promise as

a high temperature, strain tolerant, corrosion resistant coating. The cyclic integrity of bonded 0.3 or 1.2-mm-thick layers indicate a robustness compared to other oxidation-resistant coatings, the latter being typically much thinner at ~0.1 mm or less. Complex interfacial reaction layers were produced during hot pressing at 1100 °C. About 10 μm of β-Ni(Co)Al formed, decorated with various γ′ $(Ni,Co)_3Al$, Ta(Ti,Nb)C, and $W(Cr,Mo)_3B_2$ precipitates formed near the bond interface. The constituent phases and microstructures were reminiscent of those produced in aluminized superalloy coatings. On the Cr_2AlC side, an additional ~40-μm reaction zone of Cr_7C_3 formed in an interconnected network with β-Ni(Co)Al. This transitioned into a dense Cr_7C_3 Al-depletion zone, similar to that formed by Al-depletion during high temperature oxidation.

Little if any additional growth occurred after extensive exposure to 800 °C, i.e. near the expected maximum service temperature for this application, although the detailed morphology changed. The ability of MAX phases to deform without cracking may provide some strain tolerance and fatigue benefit as a coating. However, the (brittle) NiAl diffusion zone may limit this benefit because of its known fatigue debit as a coating for superalloys. The occurrence of some TCP σ-phase in the LSHR side is another cause of concern. However, it is believed that lower processing temperatures associated with overlay coatings (i.e. below 1100 °C) will greatly decrease these detrimental diffusion effects.

Oxidation of Cr_2AlC is extremely slow at 800 °C and should pose no problem for surface degradation. As a carbide, a MAX phase coating should also reduce oxygen diffusion and oxygen-induced gas phase embrittlement (GPE) of the underlying alloy. Cr_2AlC is an alumina/chromia former with no Ni or Co exposed to the environment. Therefore, Type II low temperature hot corrosion, triggered by the formation of Ni–Co–Na sulfate eutectics, is also expected to be minimal for Cr_2AlC.

Acknowledgements

The authors are grateful to Donald Humphrey for hot pressing and Joy Buehler for metallography. The helpful comments from Drs. T. Gabb and I. Locci are appreciated. This work has been supported by the Fixed Wing Project of the NASA Fundamental Aeronautics Program.

References

[1] Barsoum M. W., El-raghy T. The MAX phases : unique new carbide and nitride materials. *Am. Sci.* **2001**;*89*(July-August):334–343.
[2] Eklund P., Beckers M., Jansson U., Högberg H., Hultman L. The Mn + 1AXn phases: materials science and thin-film processing. *Thin Solid Films* **2010**;*518*(8):1851–1878. DOI: 10.1016/j.tsf.2009.07.184.
[3] Tallman D. J., Anasori B., Barsoum M. W. A critical review of the oxidation of Ti_2AlC, Ti_3AlC_2 and Cr_2AlC in air. *Mater Res Lett* **2013**;*1*(3):115–125. DOI: 10.1080/21663831.2013.806364.
[4] Tian W., Wang P., Kan Y., Zhang G. Oxidation behavior of Cr_2AlC ceramics at 1,100 and 1,250 °C. *J. Mater. Sci.* **2008**;*43*(8):2785–2791. DOI: 10.1007/s10853-008-2516-2.
[5] Lin Z. J., Li M. S., Wang J. Y., Zhou Y. C. High-temperature oxidation and hot corrosion of Cr_2AlC. *Acta Mater.* **2007**;*55*(18):6182–6191. DOI: 10.1016/j.actamat.2007.07.024.
[6] Lee D. B., Nguyen T. D., Han J. H., Park S. W. Oxidation of Cr_2AlC at 1300 °C in air. *Corros. Sci.* **2007**;*49*(10):3926–3934. DOI: 10.1016/j.corsci.2007.03.044.
[7] Smialek J. L. Oxygen diffusivity in alumina scales grown on Al-MAX phases. *Corros. Sci.* **2015**;*91*:281–286. DOI: 10.1016/j.corsci.2014.11.030.
[8] Smialek J. L. Diffusivity in alumina scales grown on Al-MAX phases. *NASA TM 2014–218344*. **2014**;(August):1–10. http://sti.nasa.gov.
[9] Lee D. B., Park S. W. Corrosion of Ti_3AlC_2 at 800–1100 °C in Ar–0.2% SO2 gas atmosphere. *Corros. Sci.* **2011**;*53*(8):2645–2650. DOI: 10.1016/j.corsci.2011.05.001.
[10] Lee D. B., Nguyen T. D., Park S. W. Corrosion of Cr_2AlC in Ar/1%SO2 gas between 900 and 1200 °C. *Oxid Met* **2011**;*75*(5–6):313–323. DOI: 10.1007/s11085-011-9233-y.
[11] Lin Z., Zhou Y., Li M., Wang J. Hot corrosion and protection of Ti_2AlC against Na_2SO_4 salt in air. *J Eur Ceram Soc* **2006**;*26*(16):3871–3879. DOI: 10.1016/j.jeurceramsoc.2005.12.004.
[12] Lin Z., Zhou Y., Li M., Wang J. Improving the Na_2SO_4-induced corrosion resistance of Ti_3AlC_2 by pre-oxidation in air. *Corros. Sci.* **2006**;*48*(10):3271–3280. DOI: 10.1016/j.corsci.2005.11.005.
[13] Walter C., Sigumonrong D. P., El-Raghy T., Schneider J. M. Towards large area deposition of Cr_2AlC on steel. *Thin Solid Films*. **2006**;*515*(2):389–393. DOI: 10.1016/j.tsf.2005.12.219.
[14] Gulbiski W. Ti–Si–C sputter deposited thin film coatings. *Surf Coating Tech.* **2004**;*180–181*:341–346. DOI: 10.1016/j.surfcoat.2003.10.084.
[15] Hajas D. E., to Baben M., Hallstedt B., Iskandar R., Mayer J., Schneider J. M. Oxidation of Cr_2AlC coatings in the temperature range of 1230 to 1410°C. *Surf Coating Tech.* **2011**;*206*(4):591–598. DOI: 10.1016/j.surfcoat.2011.03.086.
[16] Wang Q. M., Flores Renteria A., Schroeter O., Mykhaylonka R., Leyens C., Garkas W., Baben M. Fabrication and oxidation behavior of Cr_2AlC coating on Ti6242 alloy. *Surf Coating Tech.* **2010**;*204*(15):2343–2352. DOI: 10.1016/j.surfcoat.2010.01.002.
[17] Wang Q. M., Mykhaylonka R., Flores Renteria A., Zhang J. L., Leyens C., Kim K. H. Improving the high-temperature oxidation resistance of a β–γ TiAl alloy by a Cr_2AlC coating. *Corros. Sci.* **2010**;*52*(11):3793–3802. DOI: 10.1016/j.corsci.2010.07.031.
[18] Li J. J., Li M. S., Xiang H. M., Lu X. P., Zhou Y. C. Short-term oxidation resistance and degradation of Cr_2AlC coating on M38G superalloy at 900–1100 °C. *Corros. Sci.* **2011**;*53*(11):3813–3820. DOI: 10.1016/j.corsci.2011.07.032.
[19] Woodford D. A. Gas phase embrittlement and time dependent cracking of nickel based superalloys. *Energ Mater. Mater. Sci. Eng. Energ Syst.* **2006**;*1*:59–79. DOI: 10.1179/174892306X99679.
[20] Birbilis N., Buchheit R. G. Measurement and discussion of low-temperature hot corrosion damage accumulation upon nickel-based superalloy Rene 104. *Metall Mater Trans A* **2008**;*39*(13):3224–3232. DOI: 10.1007/s11661-008-9662-7.
[21] Sudbrack C., Draper S., Gorman T., Telesman J., Gabb T., Hull D. Oxidation and the effects of high temperature exposures on notched fatigue life of an advanced powder metallurgy disk superalloy. In: E. Huron, R. Reed, M. Mills, R. Montero, P. Portella JT, eds. *Superalloys 2012: 12th International Symposium on Superalloys*. Seven Springs PA: TMS, Warrendale, PA; **2012**:863–872.
[22] Encinas-Oropesa A., Drew G. L., Hardy M. C., Leggett A. J., Nicholls J. R., Simms N. J. Effects of oxidation and hot corrosion in a nickel disc alloy. *Superalloys 2008 (Eleventh Int Symp.* **2008**:609–618. DOI: 10.7449/2008/Superalloys_2008_609_618.
[23] Sumner J., Encinas-Oropesa A., Simms N. J., Oakey J. E. High temperature oxidation and corrosion of gas turbine component materials in burner rig exposures. *Mater High Temp* **2011**;*28*(4):369–376. DOI: 10.3184/096034011X13198126967382.
[24] Karabela A., Zhao L. G., Tong J., Simms N. J., Nicholls J. R., Hardy M. C. Effects of cyclic stress and temperature on oxidation damage of a nickel-based superalloy. *Mater. Sci. Eng. A* **2011**;*528*(19–20):6194–6202. DOI: 10.1016/j.msea.2011.04.029.
[25] Sato A., Chiu Y.-L., Reed R. C. Oxidation of nickel-based single-crystal superalloys for industrial gas turbine applications. *Acta Mater.* **2011**;*59*(1):225–240. DOI: 10.1016/j.actamat.2010.09.027.
[26] Moverare J. J., Johansson S. Damage mechanisms of a high-Cr single crystal superalloy during thermomechanical fatigue. *Mater. Sci. Eng. A* **2010**;*527*(3):553–558. DOI: 10.1016/j.msea.2009.08.023.
[27] Cruchley S., Evans H. E., Taylor M. P., Hardy M. C., Stekovic S. Chromia layer growth on a Ni-based superalloy: sub-parabolic kinetics and the role of titanium. *Corros. Sci.* **2013**;*75*:58–66. DOI: 10.1016/j.corsci.2013.05.016.
[28] Kitaguchi H. S., Li H. Y., Evans H. E., Ding R. G., Jones I. P., Baxter G., Bowen P. Oxidation ahead of a crack tip in an advanced Ni-based superalloy. *Acta Mater.* **2013**;*61*(6):1968–1981. DOI: 10.1016/j.actamat.2012.12.017.
[29] Karabela A., Zhao L. G., Lin B., Tong J, Hardy M. C. Oxygen diffusion and crack growth for a nickel-based superalloy under fatigue-oxidation conditions. *Mater. Sci. Eng. A* **2013**;*567*:46–57. DOI: 10.1016/j.msea.2012.12.088.

[30] Kawagishi K., Harada H., Sato A., Matsumoto K. Eq coating : a new concept for SRZ-free coating systems. *Superalloys* **2008**, *2008*:761–768.
[31] Mercer C., Kawagishi K., Tomimatsu T., Hovis D., Pollock T. M. A comparative investigation of oxide formation on EQ (equilibrium) and NiCoCrAlY bond coats under stepped thermal cycling. *Surf Coating Tech.* **2011**;*205*:3066–3072. DOI: 10.1016/j.surfcoat.2010.11.026.
[32] Smialek J. L., Garg A. Microstructure and oxidation of a MAX phase/superalloy hybrid interface. *NASA TM 2014–216679*. **2014**;(July):1–19.
[33] Gabb T. P., Gayda J., Telesman J., Kantzos P. T. Thermal and mechanical property characterization of the advanced disk alloy LSHR. *NASA TM 2005–213645*. **2005**;(June):1–75.
[34] Gabb T. P., Miller D. R. Formation of minor phases in a nickel-based disk superalloy. *NASA TM 2012–217604*. **2012**;(July):1–31.
[35] Gabb T. P., Sudbrack C. K., Draper S. L., MacKay R. A., Telesman J. Effects of long term exposures on fatigue of PM disk superalloys. *Mater Perform Charact.* **2014**;*3*(2):1–24. DOI: 10.1520/MPC20130037.
[36] Goward G. W., Boone D. H. Mechanisms of formation of diffusion aluminide coatings on nickel-base superalloys. *Oxid Met.* **1971**;*3*:475–495. DOI: 10.1007/BF00604047.
[37] Smialek J., Lowell C. Effects of diffusion on aluminum depletion and degradation of NiAl coatings. *J. Electrochem. Soc.* **1974**;*121*:800–805. http://jes.ecsdl.org/content/121/6/800.short. Accessed December 3, 2014.
[38] Zhang Y., Haynes J. A., Wright G., Pint B. A., Cooley K. M., Lee W. Y., Liaw P. K. Effects of Pt incorporation on the isothermal oxidation behavior of chemical vapor deposition aluminide coatings. *Metall Mater Trans A.* **2001**;*32*:1727–1741. DOI: 10.1007/s11661-001-0150-6.
[39] Kim H. J., Walter M. E. Characterization of the degraded microstructures of a platinum aluminide coating. *Mater. Sci. Eng. A* **2003**;*360*:7–17. DOI: 10.1016/S0921-5093(02)00733-5.
[40] Wang D., Peng H., Gong S., Guo H. NiAlHf/Ru: promising bond coat materials in thermal barrier coatings for advanced single crystal superalloys. *Corros. Sci.* **2014**;*78*:304–312. DOI: 10.1016/j.corsci.2013.10.013.
[41] Hajas, D. E., Scholz, M., Ershov, S., Hallstedt, G. B., Palmquist, J. P., and Schneider J. M. Thermal and chemical stability of Cr_2AlC in contact with Al_2O_3 and NiAl. *Int J Mater Res* **2010**;*101*(12):1–5.

Appendix A. Phase categorization summary by zone

A large number of features in five distinct zones have been discussed. For the sake of clarity and easy comparison, a summary of the more comprehensive characterization has been constructed in Table A1. Here all the primary features are listed by zone with respect to specific EDS spectra. They are presented in sequence, top to bottom, from the superalloy, across the diffusion and reaction zones, to the Cr_2AlC (left to right in micrographs). The four subcategories of the diffusion zones correspond to (i) LSHR adjacent to the diffusion zone ($LSHR_{DZ}$), (ii) the inner diffusion zone (DZ) portions near LSHR (DZ_{LSHR}) or (iii) near Cr_2AlC ($DZ1_{Cr2AlC}$), and (iv) the predominantly Cr_7C_3 depletion layer ($DZ2_{Cr2Al}$). Characteristic EDS intensity is presented in descending order as strong, medium, or weak elemental peaks, arbitrarily designated as 50–100%, 20–50%, and $<$20% of the maximum peak height, respectively. The diffusion zone entries are for the 800 °C exposed samples and generally exhibited little or no change from the 100-h to 1000-h treatments.

Thus, in sequence, the constituents for the unaffected LSHR alloy (top) exhibit a Ni-rich matrix with low levels of all the alloying elements (Co, Cr, Al, W, Mo, Ti, C, and B). There is also a small concentration of the (Ta, Ti, Nb) MC carbides and (W, Mo, Cr) M_3B_2 borides in the as-received superalloy, as previously characterized.[34] For the exposed samples, Cr-rich TCP and a grain boundary oxide were observed in the superalloy, especially after 1000 h. The carbide and boride phases were also present in the β-Ni(Co)Al reaction zone near the superalloy (left), while only the carbide persisted on the Cr_2AlC side of the bond interface (right). Small oxide particles, assumed to be Al_2O_3, decorated the apparent original bond line in both the as-hot pressed and 100 h exposed sections, but only for the DC2 sample. An (Ni, Al)-rich phase, too fine to be clearly analyzed (~0.2 μm wide) was also present in the β-Ni(Co)Al reaction zone. It contained significant Cr (and Co), but less than that for a TCP-related phase, and was high in Ni and Al suggesting γ′-Ni_3Al, but with higher Cr. At present a more consistent identification is unavailable. The final zone is a mixture of the β-Ni(Co)Al reaction layer and the Cr_7C_3 carbide, in varying degrees. This region is populated with many large alumina particles in higher concentrations than the impurity alumina phase in the as-received Cr_2AlC. Eventually the Cr_7C_3 carbide is the only phase in contact with unaffected Cr_2AlC, which in turn contains Al_2O_3 alumina and Cr_7C_3 impurity phases in the starting material (bottom of table).

Table A1. Summary of principal features in the diffusion zone of LSHR–Cr_2AlC couples

		EDS peak height			
Location	**Description**	**High**	**Medium**	**Low**	**Proposed phase**
LSHR	matrix	**Ni, Co**	**Cr,Al**	**W,Mo,Ti**	γ/γ′
LSHR	light grey particle	Ta, Nb, Ti		C	MC
LSHR	g.b. precipitate	**Ni**		**W, Co, Cr**	γ′
LSHR	white spherical	W, Mo, Cr		Ti, Al, Ni, Co, B	M_3B_2
$LSHR_{DZ}$	matrix	**Ni, Co**	**Cr, Al**	**W, Mo,Ti**	γ/γ′
$LSHR_{DZ}$	grey oriented plate	**Cr**	**Co, Ni**	**W, Mo, Al**	**TCP**
$LSHR_{DZ}$	light circular phase	Ta, Nb, Ti		C	MC
$LSHR_{DZ}$	dark gb precipitate	Cr		Ni, Co, W, Mo	Cr_2O_3
DZ_{LSHR}	D.Z matrix	Ni, Al		Co, Cr, Ti	β-NiAl
DZ_{LSHR}	grey particle	**Ni, Al**	**Cr, Co**	**W, Mo, Ti**	**?**
DZ_{LSHR}	grey particle	Ta, Nb, Ti		C	MC
DZ_{LSHR}	white particle	W, Mo, Cr		C, B	M_3B_2
bond line	dark bond line particle	Al		O	Al_2O_3
$DZ1_{Cr2AlC}$	D.Z matrix	Ni, Al		Co, Cr, Ti	β-NiAl
$DZ1_{Cr2AlC}$	grey particle	**Ni, Al**	**Cr, Co**	**W, Mo, Ti**	**?**
$DZ1_{Cr2AlC}$	grey particle	Ti, W	Nb, Mo	C, Al	MC
$DZ2_{Cr2AlC}$	amorphic islands	Cr	W, Mo	C	Cr_7C_3
$DZ2_{Cr2AlC}$	dark particle	Al		O	Al_2O_3
$DZ2_{Cr2AlC}$	underlayer	**Ni**	**Al**	**Ti, Cr, Co**	γ/γ′
$DZ2_{Cr2AlC}$	outer D.Z. matrix	Ni, Al		Co, Cr	β-NiAl
$DZ2_{Cr2AlC}$	amorphic islands	Cr	C	Al	Cr_7C_3
Cr_2AlC	dark particle	Al		O	Al_2O_3
Cr_2AlC	light phase	Cr		C	Cr_7C_3
Cr_2AlC	matrix	Cr, Al		C	Cr_2AlC

Sequenced (top to bottom) from LSHR side, through diffusion zone, to unaffected Cr_2AlC.